Analytical Model for Low-Frequency Transmission Loss Calculation of Zero-Prestressed Plates With Arbitrary Mass Loading

William T. Edwards[1], Chia-Ming Chang[2], Geoffrey McKnight[2], Steven R. Nutt[1*]

[1]M.C. Gill Composites Center, Department of Chemical Engineering and Materials Science, University of Southern California, 3651 Watt Way VHE-602, Los Angeles, CA 90089-0241, USA

[2] HRL Laboratories, 3011 Malibu Canyon Road, Malibu, CA 90265

* E-mail: nutt@usc.edu

Abstract: As the importance of sound attenuation through weight-critical structures has grown and mass law based strategies have proven impractical, engineers have pursued alternative approaches for sound attenuation. Membrane-type acoustic metamaterials have demonstrated sound attenuation significantly higher than mass law predictions for narrow, tunable bandwidths. Similar phenomena can be achieved with plate-like structures. This paper presents an analytical model for the prediction of transmission loss through rectangular plates arbitrarily loaded with rigid masses, accommodating any combination of clamped and simply supported boundary conditions. Equations of motion are solved using a modal expansion approach, incorporating admissible eigenfunctions given by the natural mode shapes of single-span beams. The effective surface mass density is calculated and used to predict the transmission loss of low-frequency sound through the plate–mass structure. To validate the model, finite element results are compared against analytical predictions of modal behavior and shown to achieve agreement. The model is then used to explore the influence of various combinations of boundary conditions on the transmission loss properties of the structure, revealing that the symmetry of plate mounting conditions strongly affects transmission loss behavior and is a critical design parameter. [DOI: 10.1115/1.4042927]

Please cite the article as: W Edwards, CM Chang, G McKnight, and SR Nutt **"Analytical model for low-frequency transmission loss calculation of plates with arbitrary mass loading",** J Vibration & Acoust (2019) DOI:10.1115/1.4042927

1. INTRODUCTION:

The attenuation of low-frequency sound through weight-critical structures has historically been a challenging task. Noise reduction approaches using traditional engineering materials typically rely on increasing the mass of acoustic barriers (the acoustic mass law), but this is an especially inefficient mechanism for attenuation of low frequency sound waves [1]. Recently developed membrane-type acoustic metamaterials (MAMs), however, have been shown, both theoretically and experimentally, to attenuate substantially more energy than mass law predictions for the low-frequency regime (100–1000 Hz) [2]. These structures are quasi-planar and comprise a membrane under tension with fixed boundaries, loaded with one or more masses. As with other locally resonant sonic materials, MAMs exhibit negative dynamic mass at acoustic excitation wavelength regimes larger than the characteristic length of the membrane structure itself, and this behavior manifests unique transmission minima and maxima within the low-frequency domain [2,3]. The frequency response of MAMs is known to be governed by the geometry, density, and tension of the membrane, and by the weight, location, and geometry of attached masses [4,5,6]. The effects of stacking multiple layers of MAMs and creating twodimensional arrays with multiple membrane-mass cells reportedly alter the bandwidth, amplitude, and the number of the transmission loss minima and maxima [7].

As efforts to scale up MAMs are undertaken, the need for efficient predictive tools increases. Finite element models of MAM vibroacoustic behavior achieve acceptable agreement with experimental measurements. However, the implementation of such models is complex and generally does not complement automated analysis and optimization. This is especially true when geometric parameters are to be varied, as this requires successively recreating the mesh on which the finite element is defined. Analytical techniques for predicting

Please cite the article as: W Edwards, CM Chang, G McKnight, and SR Nutt **"Analytical model for low-frequency transmission loss calculation of plates with arbitrary mass loading",** J Vibration & Acoust (2019) DOI:10.1115/1.4042927

transmission loss through acoustic metamaterials, in contrast, offer a more manageable implementation that meaningfully improves optimization efficiency.

Analytical modeling of sound transmission through membranes was initially explored by Ingard [8], who described transmission through a pretensioned, uniform, circular membrane and recognized the potential for using such structures as weight-efficient acoustic insulation. Around the same time, the influence of rigidly attached masses on the eigenfrequencies of vibrating membranes was also being explored [9,10]. Interest in analytical modeling of sound transmission through mass-loaded membranes, however, was not pursued until after extensive experimental and finite element data had demonstrated that such structures hold promise for weight efficient, low-frequency sound insulation.

Analytical modeling efforts have culminated in a model proposed by Chen et al. [11] that uses a point matching approach, considers the coupling of the membrane with the surrounding acoustic fluid, and offers accuracy at arbitrarily high frequency. The model accommodates both circular and rectangular membranes with an arbitrary number of masses. This method, however, (1) results in a nonlinear eigenvalue problem, and (2) requires repeated numeric integration of Green's function across the membrane surface to solve the acoustic wave equation. Executing each of these operations is computationally cumbersome and slow. To avoid these inefficient operations, Langfeldt et al. [12] presented a model in which membrane displacement is expanded in the eigenmodes of the unloaded membrane, creating a linear eigenvalue problem that is efficiently solved. Normal incidence transmission loss is approximated at low frequency by determining the effective surface mass density, which does not require numerical integration. In the low-frequency regime (wavelengths smaller than the characteristic dimension of the membrane), this model remains the most accurate and efficient method for optimizing transmission loss through MAMs.

Please cite the article as: W Edwards, CM Chang, G McKnight, and SR Nutt **"Analytical model for low-frequency transmission loss calculation of plates with arbitrary mass loading",** J Vibration & Acoust (2019) DOI:10.1115/1.4042927

As engineers continue to explore optimization of MAM structures, stiffer materials have been considered for use as the "membrane" component of MAMs. Several analytic models have been developed to describe sound transmission through single- and double-panel barriers [13,14]. These models accurately describe transmission through plates where all boundaries are clamped or all boundaries are simply supported; however, they do not accommodate plates with a combination of clamped and simply supported boundaries. Further, as presented, these models do not incorporate the influence of one or more masses bonded to either panel. Such a capability is desirable because the presence, size, and location of bonded masses give designers the ability to tune the frequencies of transmission loss maxima and minima.

To accommodate the addition of a mass bonded to a stiff acoustic barrier, Chen et al. [15] presented an analytical model describing transmission through a rectangular, pretensioned Kirchhoff–Love plate. The model achieves reasonable agreement with finite element predictions, but suffers the same numerical inefficiencies present in their membrane model [11]. Namely, it requires solving a nonlinear eigenvalue problem and repeated numerical integration. Furthermore, the model (1) applies only to rectangular membranes clamped along all four edges, (2) requires doubly symmetric mass placement, and (3) captures only doubly symmetric plate motion.

The work presented herein aims to overcome the numerical inefficiencies and limitations of the Chen plate model by adapting the numerical framework presented by Langfeldt et al. [12] to describe transmission through mass-loaded plates. Specifically, although the influence of prestress is not considered, the model presented herein avoids requiring the solution of a nonlinear eigenvalue problem. Instead, the model takes advantage of a long history of optimized standard eigenvalue solvers to find solutions to a linear eigenvalue problem. By avoiding the need to solve a nonlinear eigenvalue problem, the model

offers substantially faster computational times than the plate model presented by Chen et al. Further, the model presented herein avoids the repeated numerical integration of Green's function required in the model presented by Chen et al., streamlining an otherwise time-consuming operation.

In addition to improvements in numerical efficiency, the model presented herein accurately captures the behavior of a wider variety of mass-loaded plates. While previous work has accommodated only clamped boundary conditions, the model presented in this work accommodates any combination of clamped and simply supported edges. This is especially important to designers who may not be able to achieve perfect clamping on all plate edges in realistic deployment situations. Indeed, we show that when a clamped edge is opposite a simply supported edge, plate metamaterial behavior can exhibit additional transmission loss minima as compared with plates with uniform fastening. An additional advantage over Chen's plate model is that the symmetry requirements imposed on mass placement location are relaxed. Instead of requiring that masses be placed such that there is symmetry across both the plate midlines, the model presented here accommodates an arbitrary number of masses placed at any location on the plate with no symmetry requirements. Further, while the Chen model only predicted modal behavior that was symmetric across both plate midplanes, the model presented herein can accurately predict asymmetric modal behavior, which is critical for an accurate prediction of transmission loss for plates that do not have identical boundary conditions on all edges and for plates with eccentric mass placement.

The value of this work lies in three primary achievements. First, the model presented herein is the only analytical model to describe low-frequency sound transmission loss through plate-like acoustic metamaterials where mass placement is not limited by symmetry requirements. Second, the model accommodates various boundary conditions and combinations of boundary conditions that have hitherto been absent from the literature,

Please cite the article as: W Edwards, CM Chang, G McKnight, and SR Nutt **"Analytical model for low-frequency transmission loss calculation of plates with arbitrary mass loading",** J Vibration & Acoust (2019) DOI:10.1115/1.4042927

significantly widening the scope of acoustic transmission problems that can be addressed using analytic techniques. Finally, new insights into the influence of boundary conditions on the transmission loss through plate-like acoustic metamaterials are presented. Although the relationship between boundary conditions and frequency response of vibrating plates is well known, this work presents the first explicit demonstration of how boundary conditions influence transmission loss performance of mass-loaded plates, and reveals the critical importance of mounting conditions in determining plate-like metamaterial performance.

In the section below, we present the analytical theory describing vibration of the coupled plate–mass system and the corresponding equations of motion, the eigenfunctions used for each set of boundary conditions, the method for solving the resulting linear homogeneous eigenvalue problem, and the method for transmission loss calculation. In the Results and Discussion section, we validate the model by comparison with results obtained using established analytical and finite element techniques, and use the model to investigate the influence of boundary conditions on the transmission loss profile of plate–mass structures. We demonstrate that asymmetric mounting gives rise to additional transmission loss maxima and minima when compared with symmetric boundary conditions.

Theory:

Consider a homogeneous isotropic plate of dimensions L_x and L_y, surface mass density m′, and bending stiffness T. Bonded to the plate is a rigid inertial inclusion of mass M of arbitrary shape, the center of mass of which is located according to $[x_M, y_M]$ in the $\{\vec{x}, \vec{y}, \vec{z}\}$ coordinate frame. As shown in Figure 1, the origin is located at one corner of the plate, the positive x- and y-axes along the plate edges. The out-of-plane displacement of the plate is a function of position and time given by w(x, y, t), and the vibration of the plate is described according to the Kirchhoff–Love plate theory written as

$$m'\frac{\partial^2}{\partial t^2}w(x,y,t) + T\nabla^2\nabla^2 w(x,y,t) = P(x,y,t) + f'(x,y,t) \quad (1)$$

where $\nabla^2 = \partial^2/\partial x^2 + \partial^2/\partial y^2$ is the Laplace operator in Cartesian coordinates, P(x, y, t) is the acoustic pressure acting on the plate, and f ′(x, y, t) is the coupling force resulting from inertial inclusions mounted to the plate. Assuming harmonic time dependence and normally incident acoustic excitation, we can write

$$w(x, y, t) = \hat{w}(x, y)e^{i\omega t} \quad (2)$$

$$P(x, y, t) = \hat{P}(x, y)e^{i\omega t} \quad (3)$$

$$f'(x, y, t) = \hat{f}'(x, y)e^{i\omega t} \quad (4)$$

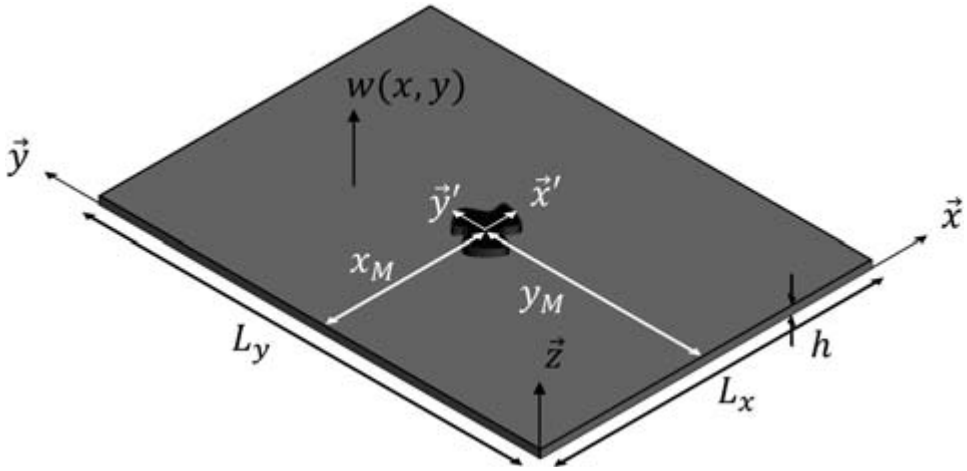

Figure 1. Definition of geometric and mathematical variables for modeling plate behavior

For the sake of brevity, the time dependence of these terms will be omitted from the mathematical expressions below. We can also introduce the dimensionless parameters given by

$$\xi = x/L_x \qquad \eta = y/L_y \qquad \zeta = z/L_x \qquad u = \hat{w}/L_x$$

$$\Lambda = L_x/L_y \qquad \beta = \hat{P}L_x/T \qquad k^2 = m'\omega^2 L_x^2/T \qquad \gamma = \hat{f}'/(TL_x) \quad (5)$$

to simplify Eq. (1) into the following form:

$$-k^2 u + \frac{\partial^4 u}{\partial \xi^4} + 2\Lambda^2 \frac{\partial^4 u}{\partial \xi^2 \partial \eta^2} + \Lambda^4 \frac{\partial^4 u}{\partial \eta^4} = \beta + \gamma \quad (6)$$

Please cite the article as: W Edwards, CM Chang, G McKnight, and SR Nutt **"Analytical model for low-frequency transmission loss calculation of plates with arbitrary mass loading",** J Vibration & Acoust (2019) DOI:10.1115/1.4042927

We next approximate the influence of the inertial inclusions. To do so, we employ a point matching approach where the coupling force that is applied over a continuous domain is approximated as a set of I forces that act at discrete points within and on the boundary of the domain of the inclusion. With this in mind, the coupling force can be expressed as

$$\gamma = \sum_{i=1}^{I} \gamma_i \delta(\xi - \xi_i)\, \delta(\eta - \eta_i) \tag{7}$$

where γ_i is the dimensionless coupling force contributed by the i^{th} collocation point, and δ is the Dirac delta function. We choose to solve the resulting equation of motion using a modal expansion approach, approximating the response of the system as a finite linear combination of N eigenfunctions $\Phi_i(\xi, \eta)$, $i=\{1, 2, \ldots, N\}$, which are determined by the boundary conditions and Cartesian geometry of the system.

Boundary Conditions and Eigenfunctions. The eigenfunction $\Phi_n(\xi, \eta)$ can be separated into the product of two dimensionally independent functions: $\Phi_n(\xi,\eta) = \phi_{n_x}(\xi)\, \phi_{n_y}(\eta)$. The index n then runs from 1 to $N = N_x N_y$, where N_x and N_y are the number of eigenfunction expansion terms used in each of the $\vec{x}$ and $\vec{y}$ dimensions. The indices n_x and n_y are determined such that $n = N_y(n_x - 1) + n_y$. The functions ϕ_{n_x} and ϕ_{n_y} are determined by the boundary conditions in each corresponding dimension (e.g., ϕ_{n_x} is determined by the boundary conditions at $x = 0$ and $x = L_x$). Equation (8) gives these expressions, where SS and CC indicate opposing boundaries that are both simply supported and clamped, respectively, and CS indicates one boundary is clamped and the other is simply supported.

$$\phi_k(\xi) = \begin{cases} \sin(a_k \xi), & \text{SS} \\ \cosh(a_k \xi) - \cos(a_k \xi) - b_k(\sinh(a_k \xi) - \sin(a_k \xi)) & \text{CC or CS} \end{cases} \tag{8}$$

The coefficients a_k are the nontrival solutions to the characteristic equation associated with each set of boundary conditions given by Eq. (9) [16]

$\sin(a_k) = 0$ for SS

Please cite the article as: W Edwards, CM Chang, G McKnight, and SR Nutt **"Analytical model for low-frequency transmission loss calculation of plates with arbitrary mass loading",** J Vibration & Acoust (2019) DOI:10.1115/1.4042927

$\cos(a_k)\cosh(a_k)=1$ for CC

$\tan(a_k)=\tanh(a_k)$ for CS (9)

The corresponding coefficients bk are found by solving Equation (10) to ensure CC and CS eigenfunctions satisfy the appropriate boundary conditions:

$$\phi_k(\xi)|_{\xi=0,1} = \frac{d\phi_k(\xi)}{d\xi}|_{\xi=0,1} = 0 \qquad \text{for CC}$$

$$\phi_k(\xi)|_{\xi=0,1} = \frac{d\phi_k(\xi)}{d\xi}|_{\xi=0} = 0 \qquad \text{for CS} \tag{10}$$

Using the Rayleigh–Ritz method, we can approximate the unitless modal displacement as a linear combination of appropriately chosen eigenfunctions according to Equation (11)

$$u \approx \sum_{n_x=1}^{N_x}\sum_{n_y=1}^{N_y} q_n \phi_{n_x}(\xi)\phi_{n_y}(\eta) \tag{11}$$

Note that the set of eigenfunctions in the $\vec{x}$ direction, $\phi(\xi)$, does not have to be identical to the set of eigenfunctions in the $\vec{y}$ direction, $\phi(\eta)$: that is, any combination of clamped and simply supported boundaries can be studied.

Eigenvalue Problem. After substituting Eqs. (7) and (11) into Equation (6), we rearrange the summations into matrix operations of the following form:

$$(\mathbf{C} - k^2\mathbf{M})\mathbf{q} = \beta\mathbf{b} + \mathbf{L}\boldsymbol{\gamma} \tag{12}$$

where the dimensionless coupling-force vector $\boldsymbol{\gamma}$ contains entries $[\gamma 1, \gamma 2, \ldots, \gamma N]^T$, and the stiffness matrix $\mathbf{C} = (c_{mn}) \in \mathbb{R}^{N\times N}$ and the mass matrix $M = (m_{mn}) \in \mathbb{R}^{N\times N}$ have entries given by

$$c_{mn} = \begin{cases} f_{x,m}^4 + 2(g_{x,m})(\Lambda^2 g_{y,m}) + \Lambda^4 f_{y,m}^4 & for\ m = n \\ 0 & else \end{cases} \tag{13}$$

$$m_{mn} = \begin{cases} h_{x,m} & for\ m = n \\ 0 & else \end{cases} \tag{14}$$

and the coupling matrix $L=(l_{mn}) \in \mathbb{R}^{N\times I}$ and forcing vector $b = (b_n) \in \mathbb{R}^N$ have entries given by

$$l_{mn} = \phi_{n_x}(\xi_n)\,\phi_{n_y}(\eta_n) \tag{15}$$

$$b_n = d_{n_x} d_{n_y} \tag{16}$$

Please cite the article as: W Edwards, CM Chang, G McKnight, and SR Nutt **"Analytical model for low-frequency transmission loss calculation of plates with arbitrary mass loading",** J Vibration & Acoust (2019) DOI:10.1115/1.4042927

The values of the coefficients f_n, g_n, h_n, and d_n are listed in Table 1 as functions of the boundary conditions imposed on the plate.

To further constrain the system of equations (unknown term γ remains in Equation (12)), we write a separate set of equations describing the motion of the attached rigid mass in the coordinate frame $\{\vec{x}', \vec{y}', \vec{z}'\}$, centered at the center of mass of the inertial inclusion

Table 1. Coefficients of entries in C and M matrices

Coefficients for various boundary conditions				
	f_n	h_n	g_n	d_n
Clamped- Clamped	a_n	1	$b_n a_n(2- b_n a_n)$	$2b_n a_n^{-1}(1-(-1)^{-n}$
Clamped- Pinned	a_n	1	$b_n a_n(1- b_n a_n)$	$a_n^{-1}[(-1)^{n+1}\sqrt{b_n^2+1}-\sqrt{b_n^2-1}+2b_n$
Pinned- Pinned	$\frac{a_n}{\sqrt{2}}$	$\frac{1}{2}$	$\frac{a_n^2}{4}$	$\frac{1}{a_n}[1-(-1)^n]$

(Figure 1). As shown in Equation (17), the displacement anywhere within the domain of the inclusion can be described using the position of the center of mass, u_A, C_M, and two terms, $\alpha_{\xi'}$ and $\alpha_{\eta'}$, describing rotation about the $\vec{x}'$ and $\vec{y}'$ axes, respectively,

$$u_M(\xi',\eta') = u_{M,CM} - \alpha_\eta \xi' + \frac{1}{\wedge}\alpha_\xi \eta' \quad (17)$$

Equation (17) is rearranged by expressing u_M,C_M as a function of the dimensionless frequency parameter k, the dimensionless mass parameter μ = M/(m′L_x^2), and the point-force coupling terms γ_i according to

$$u_{M,CM} = \frac{1}{\mu k^2}\sum_{i=1}^{I}\gamma_i \quad (18)$$

where M is the total mass of the inertial inclusion mounted on the plate. We can similarly express the rotational terms α_ξ and α_η as shown below, where dimensionless rotational inertia

Please cite the article as: W Edwards, CM Chang, G McKnight, and SR Nutt **"Analytical model for low-frequency transmission loss calculation of plates with arbitrary mass loading",** J Vibration & Acoust (2019) DOI:10.1115/1.4042927

parameters are normalized according to $\vartheta_\xi = J_{x'}/(ML_x^2)$ and $\vartheta_\eta = J_y/(ML_x^2)$, and $J_{x'}$ and $J_{y'}$ are moments of inertia about the $\overrightarrow{x'}$ and $\overrightarrow{y'}$ axes.

$$\alpha_\xi = \frac{1}{\mu k^2 \wedge \vartheta_\eta} \sum_{i=1}^{I} \xi'_i \gamma_i \tag{19}$$

$$\alpha_\eta = \frac{1}{\mu k^2 \vartheta_\eta} \sum_{i=1}^{I} \eta'_i \gamma_i \tag{20}$$

Using these relations, we can rewrite Equation (17) as

$$u_A(\xi', \eta') = \frac{1}{\mu k^2} \sum_{i=1}^{I} \left(1 + \frac{\xi' \xi'_i}{\vartheta_\eta} + \frac{\eta' \eta'_i}{\wedge^2 \vartheta_{\xi^*}}\right) \gamma_i \tag{21}$$

Because the inertial inclusion is perfectly bonded to the plate, we have mathematically identical motion in the plate and inclusion at each of the collocation points, implying

$$u_A\left(\xi'_m \eta'_m\right) = u(\xi_m \eta_m) \text{ for } 1 \le m \le I \tag{22}$$

which can be written in the matrix form according to

$$-\mathbf{L}^T \mathbf{q} + \frac{1}{k^2} \mathbf{G} \boldsymbol{\gamma} = 0 \tag{23}$$

where the matrix $G = (g_{mn}) \in \mathbb{R}^{I \times I}$ has entries given by

$$g_{mn} = \frac{1}{\mu}\left(1 + \frac{\xi' \xi'_i}{\vartheta_\eta} + \frac{\eta' \eta'_i}{\wedge^2 \vartheta_\xi}\right) \tag{24}$$

We can now combine Equations (12) and (23) into a single block matrix system of the following form:

$$\begin{bmatrix} \boldsymbol{C} - k^2 \boldsymbol{M} & -\boldsymbol{L} \\ -\boldsymbol{L}^T & \boldsymbol{G}/k^2 \end{bmatrix} \begin{bmatrix} \boldsymbol{q} \\ \boldsymbol{\gamma} \end{bmatrix} = \beta \begin{bmatrix} \boldsymbol{b} \\ 0 \end{bmatrix} \tag{25}$$

the homogeneous form for which can be expressed as the generalized eigenvalue problem given by

$$\mathbf{A}\mathbf{x} = k^2 \mathbf{B}\mathbf{x} \tag{26}$$

where

$$\mathbf{A} = \begin{bmatrix} \boldsymbol{C} & -\boldsymbol{L} \\ 0 & \boldsymbol{G} \end{bmatrix}, \mathbf{B} = \begin{bmatrix} \boldsymbol{M} & 0 \\ \boldsymbol{L}^T & 0 \end{bmatrix}, \text{ and } \mathbf{x} = \begin{bmatrix} \boldsymbol{x}_q \\ \boldsymbol{x}_\gamma \end{bmatrix} \tag{27}$$

Please cite the article as: W Edwards, CM Chang, G McKnight, and SR Nutt **"Analytical model for low-frequency transmission loss calculation of plates with arbitrary mass loading",** J Vibration & Acoust (2019) DOI:10.1115/1.4042927

This equation can now be solved using standard solvers to identify the first K eigenvalues (indicating modal frequencies) and eigenvectors (indicating coupling forces at collocation points and modal coefficients for eigenfunction weighting coefficients). If we assume that the deformation of the membrane under steady-state vibration can be approximated by a linear combination of the first K eigenmodes, we can write $[\,\boldsymbol{q}^T \boldsymbol{\gamma}^T\,]^T \approx \mathbf{X}\mathbf{c}(\mathrm{k})$, arranging eigenvectors into a matrix $\mathbf{X} \in \mathbb{R}^{(N+I)\times K}$, where the ith column of the matrix is the ith eigenvector of Equation (26), and $\mathrm{c} = [c_1, c_2, \ldots, c_K]^T$ is a vector containing the modal contribution factors. We can solve these modal contribution factors with inhomogeneous equation (25), using the identities in Equation (27) and pre-multiplying by the matrix X^T

$$\mathbf{X}^T\mathbf{B}\mathbf{X}\mathbf{c} - k^2\mathbf{X}^T\mathbf{B}\mathbf{X}\mathbf{c} = \beta\mathbf{X}^T\begin{bmatrix}\mathbf{b}\\0\end{bmatrix} \tag{28}$$

Using the identity $\mathrm{AX} = \mathrm{B}\mathrm{X}\Lambda$, where Λ is a diagonal matrix with entries corresponding to the first K dimensionless eigen frequencies extracted from Equation (26), we can calculate the coefficients c as a function of dimensionless frequency k according to

$$\mathbf{c}(\mathrm{k}) = \beta(\Lambda - k^2\boldsymbol{I})^{-1}(\boldsymbol{X}^T\boldsymbol{B}\boldsymbol{X})^{-1}\boldsymbol{X}^T\begin{bmatrix}\mathbf{b}\\0\end{bmatrix} \tag{29}$$

Transmission Loss. We calculate transmission through the plate under the assumption that sound radiation behavior is governed primarily by the surface-averaged vibration amplitude. This assumption is appropriate for frequencies where the acoustic wavelength λ is greater than the characteristic length of the plate $\sqrt{L_x^2 + L_y^2}$ [17]. Because we are interested primarily in low-frequency performance, this assumption is not particularly restrictive and will be discussed more thoroughly in the next section. From [12], the effective mass density of the plate can be calculated as a function of excitation frequency according to

$$\widetilde{m}' = -\frac{m'}{k^2[\boldsymbol{b}^T\,0]\boldsymbol{X}\boldsymbol{c}} \tag{30}$$

Please cite the article as: W Edwards, CM Chang, G McKnight, and SR Nutt **"Analytical model for low-frequency transmission loss calculation of plates with arbitrary mass loading",** J Vibration & Acoust (2019) DOI:10.1115/1.4042927

The effectivemass density $\tilde{m}'$ is used in accordance with the acoustic mass law to finally calculate the transmission coefficient t according to

$$\frac{1}{t} = 1 + \frac{i\omega\tilde{m}'}{2\rho_0 c_0} \tag{31}$$

where ρ_0 and c_0 are the density and speed of sound of the acoustic fluid through which sound is being transmitted. Using the transmission coefficient, transmission loss in dB can be calculated per $TL_0 = -20 \log_{10}|t|$.

2. RESULTS AND DISCUSSION

To facilitate the discussion of various boundary conditions, the following convention will be adopted for the remainder of this paper. Each edge is assigned C or S to indicate whether it is clamped or simply supported. Each plate is named according to the four letters corresponding to the conditions at each boundary. The first letter in the series corresponds to the edge at x=0, and each subsequent letter describes the adjacent edge in a counter-clockwise direction. For example, a plate with boundary conditions CCSC would be clamped at the three edges defined by x = 0, y = L_y, and y = 0 and simply supported along the edge x = L_x.

Validation. To validate the efficacy of the analytic model developed above, we compare it against two established and generally accepted approaches. In the first approach, the eigenfrequencies of plates without inertial inclusions (M=I =0) were compared with analytical results collected by Belvins [18]. All combinations of clamped and simply supported boundary conditions were considered, as were both square and rectangular plates (Λ=0.5). For N = 3600, analytical model predictions of dimensionless eigenfrequencies achieved agreement with published values, having less than 0.7% difference in all cases.

To confirm that the influence of inertial inclusions is appropriately captured, a finite element model was implemented. The plate was modeled as a thin shell comprising parabolic triangular elements. The inertial inclusion was modeled as a solid body with parabolic

Please cite the article as: W Edwards, CM Chang, G McKnight, and SR Nutt **"Analytical model for low-frequency transmission loss calculation of plates with arbitrary mass loading",** J Vibration & Acoust (2019) DOI:10.1115/1.4042927

tetrahedral elements. An element size of 0.001 m with a 5e-5 m tolerance was specified, resulting in approximately 113,000 nodes and 58,000 elements. High mesh quality was verified by examining element aspect ratios and Jacobian. The average element aspect ratio was 1.73 with a maximum aspect ratio of 3.08 and 98.3% of elements characterized by aspect ratios of less than 2. The average Jacobian was 1.0000 with a minimum of 1.0000 and a maximum of 1.0002. Boundary conditions were implemented assigning immovable or fixed restraints to simply supported and clamped plate edges, respectively. The immovable condition accommodated rotation of the edge nodes, but restricted all translation, while the fixed condition did not allow rotation or translation of edge nodes. Figure 2 shows the implementation of this finite element model for the case of CCSS boundaries with an eccentric mass located at x_M =0.12 m and y_M =0.10 m. In this figure, the simply supported boundaries are symbolized with arrows along each primary axis, indicating that edge nodes translation is constrained. Clamped edges are symbolized with flanged arrows pointing along each primary axis, indicating that edge nodes are translation and rotation constrained.

Material properties were assigned to correspond to aluminum (E = 69 GPa, ρ = 2700 kg/m^3, ν=0.33), and geometric parameters were set to L_x =L_y=0.16 m and h=0.001 m. Only one inertial inclusion was considered: a cubic body with side lengths of 0.01 m and total mass 0.011 kg, located at the center of the plate (x_M =y_M =0.08 m). The inertial inclusion was assigned material properties corresponding to pure lead (Pb) and modeled as a linear elastic body perfectly bonded to the plate. A frequency analysis was conducted and solved using the Intel Direct Sparse solver, yielding the first 20 eigenfrequencies and corresponding modal responses. Finite element data were compared to analytical predictions for a plate–mass system with corresponding material and geometric properties. Numerical parameters were given by N=3600 (N_x=N_y=60), I =16, and K =100.

Please cite the article as: W Edwards, CM Chang, G McKnight, and SR Nutt **"Analytical model for low-frequency transmission loss calculation of plates with arbitrary mass loading",** J Vibration & Acoust (2019) DOI:10.1115/1.4042927

Table 2 compares the analytic and finite element predictions for the first eight eigenfrequencies of plates with CCCC and SSSS mounting conditions. Analytical predictions achieve an accurate agreement with finite element results. The average difference between the analytic and finite element results for the first eight modes is 1.41%, with a maximum error of 4.06%. Analytic predictions for these mode shapes corresponding to these eigenfrequencies are pictured in Figure 3 for CCCC plates. Mode 3 and mode 8 are omitted from this figure as these modes are simple 90 deg rotations of modes 2 and 7, respectively. In all figures depicting modal response, solid contours indicate positive plate deflection in the z direction, and dashed contours indicate negative deflection. The brightness of contour lines correlates with deflection amplitude,

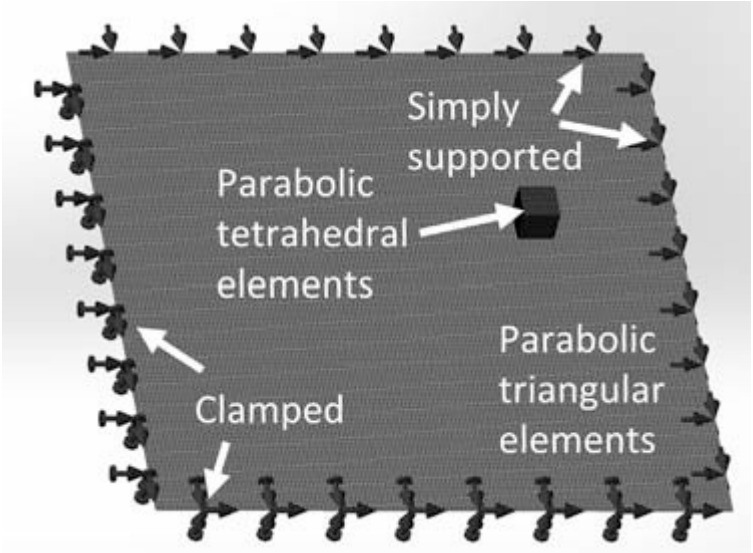

Figure 2. Finite element model implementation for the CCSS plate with eccentric mass highlighting element types and boundary conditions

Table 2 Comparison of analytic and finite element eigenfrequency predictions (centrally located mass, $\xi_{M,CM}= \eta_{M,CM}= 0.5$)

Clamped boundaries (CCCC)				Simply supported boundaries (SSSS)		
Mode Index	Analytic (Hz)	FEA (Hz)	Error (%)	Analytic (Hz)	FEA (Hz)	Error (%)
1	251.1	247.4	1.47	149.8	149.0	0.53
2	681.4	676.8	0.68	465.1	464.4	0.15
3	681.4	676.8	0.68	465.1	464.4	0.15
4	1016	974.7	4.06	726.1	713.9	1.68
5	1087	1054	3.04	773.1	767.6	0.71

Please cite the article as: W Edwards, CM Chang, G McKnight, and SR Nutt **"Analytical model for low-frequency transmission loss calculation of plates with arbitrary mass loading",** J Vibration & Acoust (2019) DOI:10.1115/1.4042927

6	1301	1279	1.69	961.1	958.0	0.32
7	1526	1481	2.95	1199	1190	0.75
8	1526	1481	2.95	1199	1190	0.75

where brighter lines indicate higher magnitude than darker lines. Clamped boundaries are indicated by a hatched region along the corresponding edge, otherwise edges are simply supported. The mode shapes captured in Figure 3 are distinct yet analogous to the corresponding shapes exhibited by plates with SSSS boundary conditions.

The modal response shapes predicted by each method similarly achieve agreement: Figure 4 shows a comparison of normalized displacement maps of modes 1, 4, and 7 generated by finite element and analytic techniques. This figure highlights consistency between the two methods for doubly symmetric plate motion—modes 1 and 4—and antisymmetric-symmetric plate motion—mode 7—about midplanes normal to $\vec{x}$ and $\vec{y}$. Because the mass was placed centrally for model verification, modal responses were exclusively symmetric and antisymmetric (for the boundary conditions considered in Table 2). However, the ability to predict both types of response confirms the absence of symmetry limitations present in the previous work.

For confidence in the ability to accurately accommodate eccentric mass placement and combinations of simply supported and clamped boundary conditions, additional data were generated for plates with eccentric mass placement (x_M = 0.12 m, y_M = 0.10 m) on plates with CCSS and CSCS boundaries. Table 3 compares analytic and finite element predictions for the first eight eigenfrequencies of such plates. Analytical predictions again achieve reasonable agreement with finite element results. The average difference between the analytic and finite element results for the first eight modes is 2.12%, with a maximum error of 3.96%.

The results verify that the analytical model presented herein accurately captures modal behavior of the mass-loaded plate. Furthermore, the model accurately captures symmetric (about both midplanes) and asymmetric plate motion, significantly relaxing symmetry

requirements present in the previous work. This aspect is particularly critical for investigating plates with dissimilar opposing boundaries (CCCS, CCSS, CSSS), for plates with multiple masses that are not characterized by symmetric loading about both midplanes (parallel to z x and y z), and for plates with a single eccentric mass.

Effect of Boundary Conditions on Vibroacoustic Properties

Modal Response. To investigate the effect of boundary conditions on the transmission loss profile of plate structures, all combinations of clamped and simply supported edges were considered. The same geometric and material parameters used to describe the plate and inertial inclusion are given in the validation section above. Table 4 compares the eigenfrequencies of analogous modes for all combinations of boundary conditions considered. Plates with fewer clamped edges exhibit lower natural frequencies (with frequencies for CCSS generally being lower than for CSCS plates). For corresponding eigenmodes, eigenfrequencies were

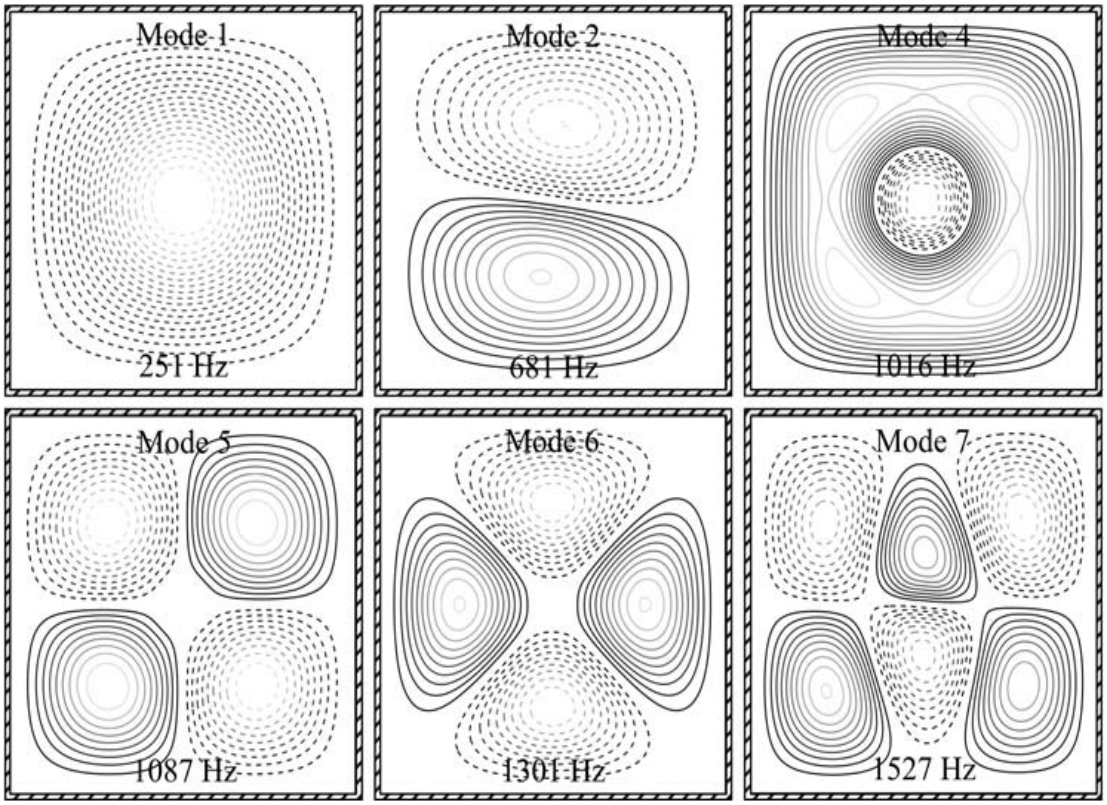

Please cite the article as: W Edwards, CM Chang, G McKnight, and SR Nutt **"Analytical model for low-frequency transmission loss calculation of plates with arbitrary mass loading",** J Vibration & Acoust (2019) DOI:10.1115/1.4042927

Fig. 3 Analytical prediction for the first six unique mode shapes of CCCC plates. Modes 3 and 8 are omitted, because they occur at the same frequency and are simple 90 deg rotations of modes 2 and 7, respectively.

20–40% lower in SSSS plates than CCCC plates. Generally, lower order modes were more strongly influenced by mounting conditions.

As the natural frequencies of this system are directly related to its stiffness, the boundary conditions studied can be ranked from the stiffest to the least stiff according to CCCC, CCCS, CSCS, CCSS, CSSS, SSSS. One notable exception to this trend is mode 4 in CCSS plates. The eigenfrequency of this mode is greater than the corresponding eigenfrequency in CSCS-mounted plates. This anomalous increase in frequency is accompanied by a corresponding change in mode shape: Figure 5 shows that, although occurring at different frequencies, nearly all plates exhibit analogous response shapes except for the CCSS plate. The unique response of the CCSS plate is attributed to the doubly mismatched nature of its opposing boundaries, giving rise to a mode shape that differs substantially from its analog in other plates.

Indeed, when discussing the influence of boundary conditions on mode shape, it is helpful to divide the boundary conditions studied into two classes. The first class we identify as Class A, defined by plates in which each pair of opposing edges is identically supported—this class includes CCCC, CSCS, and SSSS conditions. The second class we identify as Class B, in which plates have at least one pair of opposing boundaries where a clamped edge is opposite as simply supported edge—this class includes CCCS, CCS, and CSSS conditions. For improved clarity, in the remainder of this paper, each boundary condition will include a subscript indicating to which class it belongs (e.g., $CCCC_A$ belongs to Class A and $CSSS_B$ belongs to Class B).

Please cite the article as: W Edwards, CM Chang, G McKnight, and SR Nutt **"Analytical model for low-frequency transmission loss calculation of plates with arbitrary mass loading",** J Vibration & Acoust (2019) DOI:10.1115/1.4042927

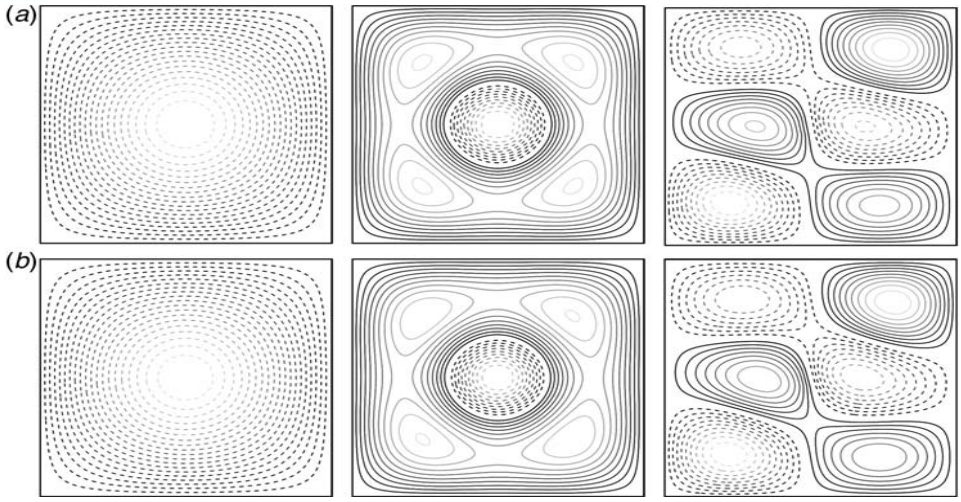

Fig. 4 Comparison of mode shapes 1, 4, and 7 (left to right) for simply supported boundaries as predicted using (a) analytic and (b) finite element techniques

Table 3 Comparison of analytic and finite element eigenfrequency predictions (eccentric mass placement, $\xi_{M,CM}$= 0.75, $\eta_{M,CM}$= 0.625)

	CCSS			CSCS		
Mode Index	Analytic (Hz)	FEA (Hz)	Error (%)	Analytic (Hz)	FEA (Hz)	Error (%)
1	214.2	211.0	1.49	251.9	247.8	1.63
2	499.8	480.0	3.96	485.7	470.9	3.05
3	583.6	575.7	1.35	585.5	574.7	1.84
4	865.9	841.7	2.79	848.9	838.0	1.28
5	1016	996.2	1.95	971.3	950.7	2.12
6	1076	1058.0	1.67	1115	1093	1.97
7	1347	1310	2.75	1295	1271	1.85
8	1405	1361	3.13	1421	1406	1.06

Table 4 Comparison of eigenfrequencies for identical plate–mass system with all combinations of clamped and simply supported boundary conditions

Mode Index	CCCC	CCCS	CSCS	CCSS	CSSS	SSSS
1	251.1	228.0	210.8	201.2	176.8	149.8
2	681.4	572.8	516.4	539.8	485.6	465.1
3	681.4	658.1	645.5	566.7	529.5	465.1
4	1016	936.7	818.6	891.7	793.1	726.2
5	1087	995.0	935.8	917.1	840.3	773.2
6	1301	1212	1186	1108	1047	961.1

indicating to which class it belongs (e.g., CCCCA belongs to Class A and CSSSB belongs to

Plates belonging to Class A produced modal responses that were all either symmetric or antisymmetric about each midplane parallel to $\vec{y}\,\vec{z}$ and $\vec{x}\,\vec{z}$. A representative example of Class A mode shapes can be seen in Figure 3 which shows the first eight modes of the CCCCA.

Please cite the article as: W Edwards, CM Chang, G McKnight, and SR Nutt **"Analytical model for low-frequency transmission loss calculation of plates with arbitrary mass loading",** J Vibration & Acoust (2019) DOI:10.1115/1.4042927

The mode shapes of CSCSA and SSSSA plates are unique but analogous to those pictured in Fig. 3. Modes 2, 3, 7, and 8 can be seen to exhibit antisymmetric responses across only one midplane of the plate, while mode 5 was characterized by antisymmetric response across each. The volume displaced during vibration on either side of these planes of antisymmetric response is equal and opposite, implying that these modes will not contribute to the transmission of acoustic energy through such plates.

For all plates belonging to Class A, only modes 1, 4, and 6 were characterized by symmetric motion across both the $\vec{y}\,\vec{z}$-midplane and the $\vec{x}\,\vec{z}$-midplane. Of these modes, only modes 1 and 4 displace a nonzero volume of acoustic fluid during vibration for all three boundary conditions. These modes for CCCCA plates can be seen in Figure 3 and mode 4 for all plates is shown in Figure 5. Figure 6 shows that mode 6 only displaces a nonzero volume for CSCSA plates. In this figure, two midplanes of anti-symmetry in CCCCA and SSSSA plates can be identified for mode 6: each plane defined by the $\vec{z}$ a line from one corner of the plate to the opposite corner. The existence of these midplanes of antisymmetric motion indicates that mode 6 will not contribute to the transmission of acoustic energy the plates with CCCCA and SSSSA boundary conditions. For CSCSA plates, however, the motion about these planes is asymmetric—but not antisymmetric—and the volume displaced during mode 6 during vibration is nonzero. Only activation of modes with nonzero volume displacement will propagate acoustic energy through the plate.

Plates belonging to Class B demonstrated modal responses that exhibit symmetric/antisymmetric motion about only one plane. For CCCSB and CSSSB cases, eigenmodes exhibit this behavior about the midplane parallel to the only pair of matching boundaries (i.e., $\vec{x}\,\vec{z}$ and $\vec{y}\,\vec{z}$, respectively). Strictly symmetric or antisymmetric modal responses, however, are not observed about the midplane parallel to the pair of mismatched boundaries. In all cases, deflection was larger on the side of the midplane corresponding to the

Please cite the article as: W Edwards, CM Chang, G McKnight, and SR Nutt **"Analytical model for low-frequency transmission loss calculation of plates with arbitrary mass loading",** J Vibration & Acoust (2019) DOI:10.1115/1.4042927

simply supported boundary than on the clamped side. In plates with CCSSB boundaries, modal responses were asymmetric about both the $\vec{x}$-$\vec{z}$- and $\vec{y}$-$\vec{z}$- midplanes, but symmetry (or anti-symmetry) was observed about the diagonal midplane containing $\vec{z}$, the origin, and the point (L_x, L_y, 0). This can be clearly seen in Figure 7 where the first six modes for CCSSB plates are pictured. Asymmetric deformation about these midplanes is explained by higher plate compliance on the simply supported side than on the clamped side, resulting in larger deformation on the simply supported side. An important implication of this asymmetry is that fewer modes oscillate with zero volume velocity. Specifically, for $CCCS_B$ boundaries, the only modes to exhibit zero net volume displacement are modes 3, 5, and 7; for $CSSS_B$ boundaries,

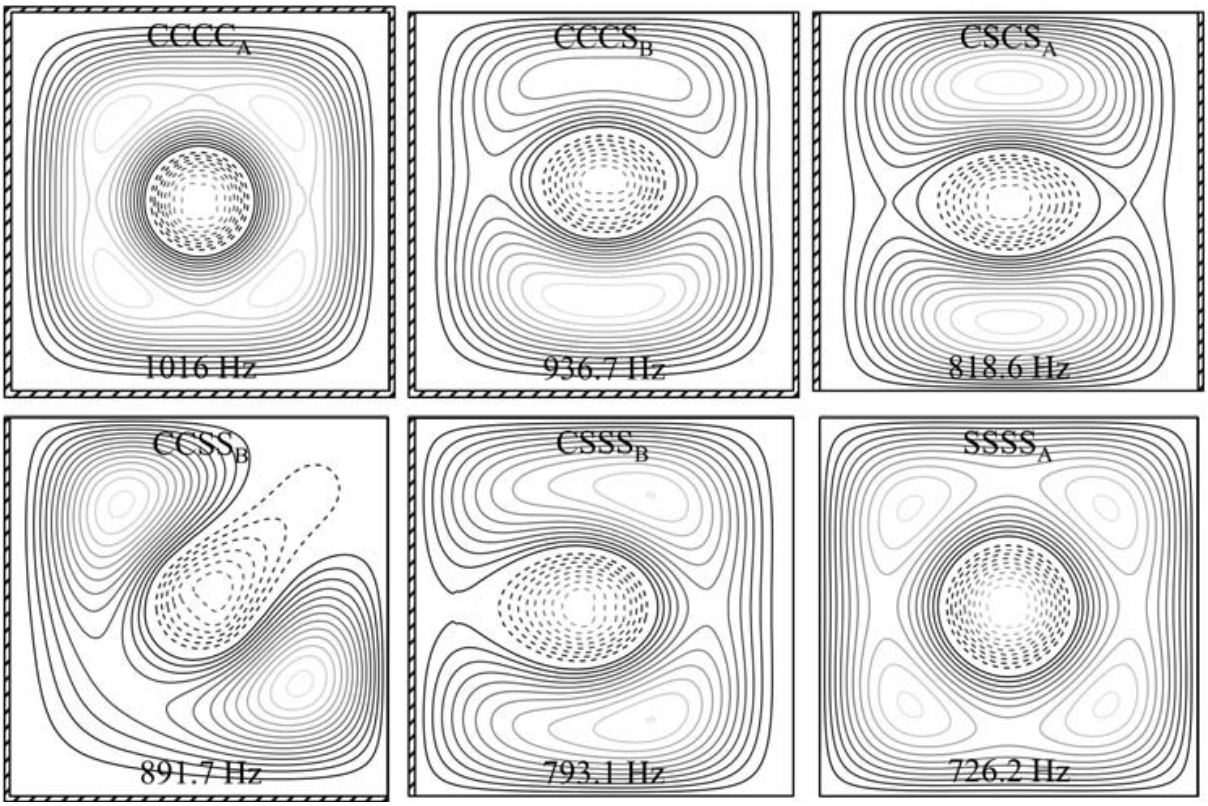

Figure 5. Comparison of normalized shapes of mode 4 for various boundary conditions

Please cite the article as: W Edwards, CM Chang, G McKnight, and SR Nutt **"Analytical model for low-frequency transmission loss calculation of plates with arbitrary mass loading",** J Vibration & Acoust (2019) DOI:10.1115/1.4042927

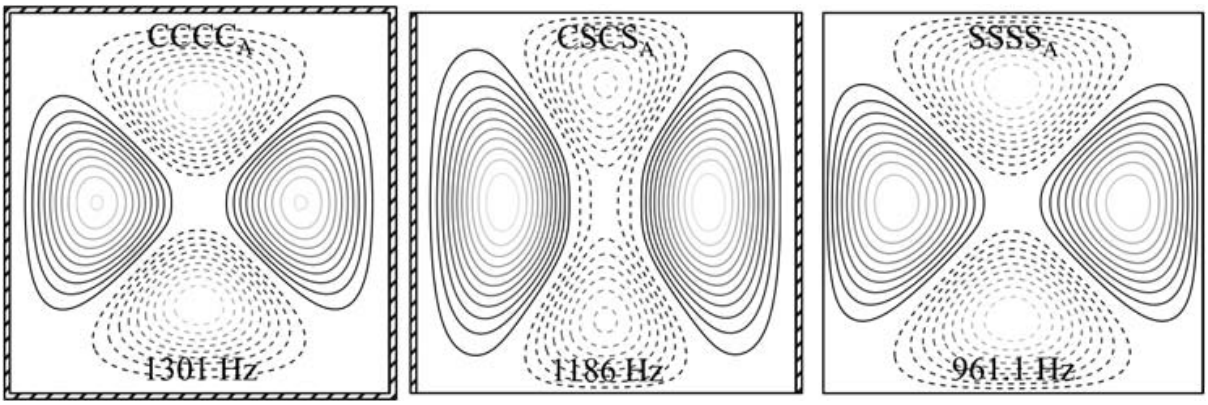

Figure 6. Comparison of mode 6 for Class A plates. CCCC and SSSS plates are characterized by an antisymmetric response that is not observed in CSCS plates.

only modes 2, 5, and 8 exhibit zero net volume displacement. This result indicates that plates belonging to Class B have a more complex transmission loss profile than plates belonging to Class A because there are more modes that propagate acoustic energy.

Transmission Loss. Figure 8 compares the transmission loss profile of a single plate–mass system with each type of boundary condition in Class A. The frequency range considered spans 10–2000 Hz, although the assumptions presented in the Theory section are only satisfied for frequencies less than 1515 Hz. Fortunately, frequencies of primary interest for targeted acoustic treatments (between modes 1 and 4) are captured accurately for the plate sizes studied. In all cases, there is a transmission loss minimum at the frequency of the first mode. First, as the number of clamped boundary conditions decreases, the maxima and minima of the transmission profile are shifted to lower frequency ranges, a result that is consistent with the trend evident in Table 4. Further, the transmission loss through the structure at frequencies below the first mode where acoustic transmission is stiffness dominated is indeed strongly influenced by the boundary conditions of the plate: more compliant mounting conditions result in significantly larger displacements and hence higher acoustic transmission, leading to differences of up to 12 dB.

Please cite the article as: W Edwards, CM Chang, G McKnight, and SR Nutt **"Analytical model for low-frequency transmission loss calculation of plates with arbitrary mass loading",** J Vibration & Acoust (2019) DOI:10.1115/1.4042927

Note that the first two minima in Figure 8 for all cases correspond to the frequencies of modes 1 and 4 from Table 4, and no features indicate any influence of modes 2, 3, 5, 7, or 8 on any curve. In the cases of CCCCA and SSSSA plates, mode 6 also appears to have no influence on the transmission properties; however, for CSCSA plates, this is not true. Figure 8 shows that for CSCSA plates, an additional transmission loss minimum and maximum exist in the vicinity of mode 6 (at 1186 Hz). These additional features arise from the mismatched boundary conditions, which promote a modal response that has nonzero volumetric displacement across the xy-plane and increases transmission efficiency. In the cases with CCCCA and SSSSA boundaries, the symmetry of boundary conditions ensures the corresponding mode has zero net displacement.

A similar effect can be seen in the class of asymmetric boundary conditions. Figure 9 shows the transmission loss performance of the remaining plate–mass systems studied, from which it is apparent that the vibroacoustic behavior of systems with asymmetric mounting conditions is considerably more complex than systems with symmetric boundaries. In the case of symmetric boundaries, many eigenmodes have zero net displacement across the xy-plane. However, the corresponding modes in plates with asymmetric boundaries result in small, but nonzero, displacements, yielding efficient transmission at these frequencies.

When Figure 8 is compared against Figure 9, the importance of ensuring that the prescribed boundary conditions are enforced is evident. Even one insufficiently clamped boundary results in a sharp transmission loss dip with 100 Hz bandwidth at a frequency near

Please cite the article as: W Edwards, CM Chang, G McKnight, and SR Nutt **"Analytical model for low-frequency transmission loss calculation of plates with arbitrary mass loading",** J Vibration & Acoust (2019) DOI:10.1115/1.4042927

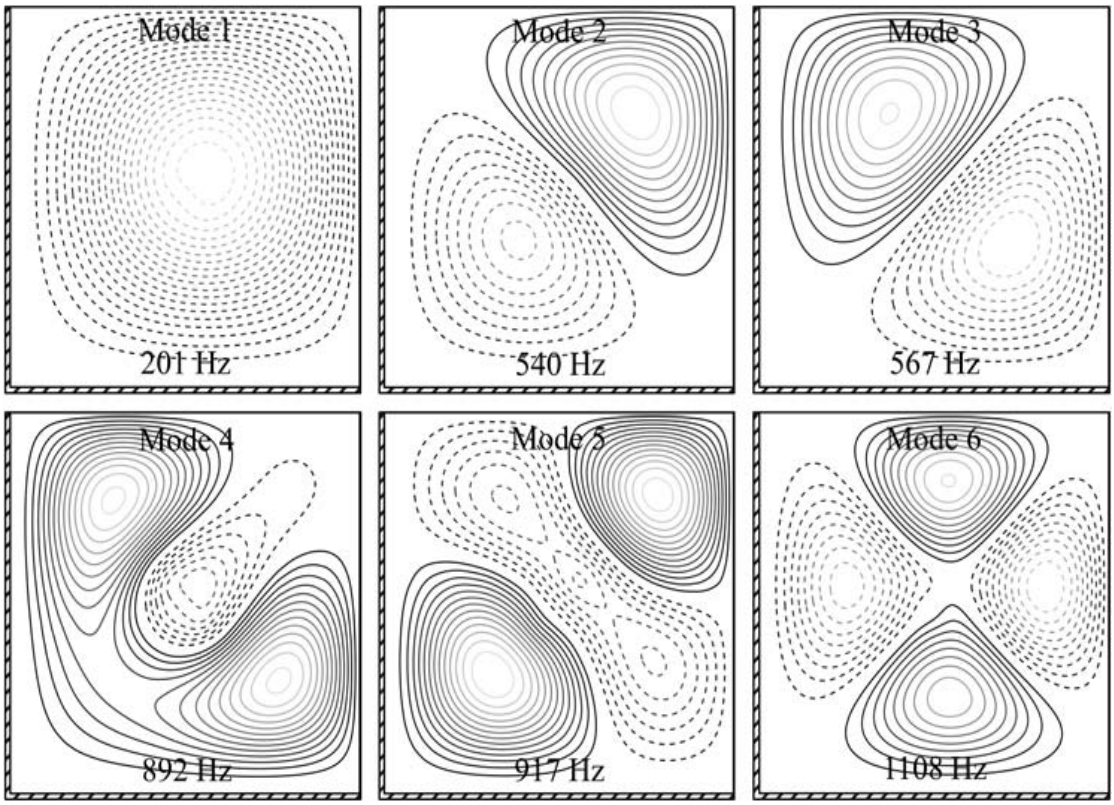

Figure 7. Analytical prediction for the first six mode shapes of CCSS plates

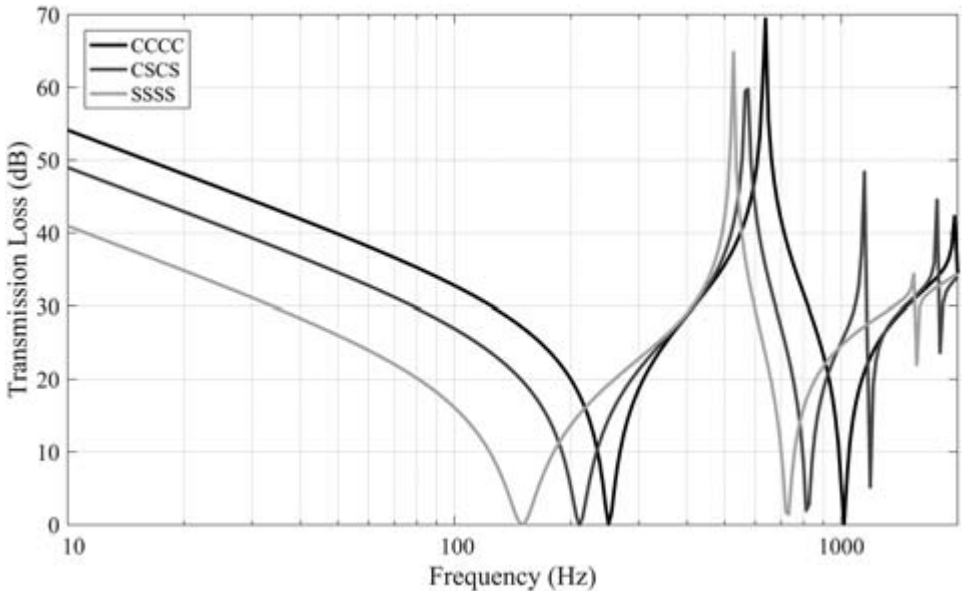

Figure 8. Transmission loss through plates belonging to Class A as a function of frequency

Please cite the article as: W Edwards, CM Chang, G McKnight, and SR Nutt **"Analytical model for low-frequency transmission loss calculation of plates with arbitrary mass loading",** J Vibration & Acoust (2019) DOI:10.1115/1.4042927

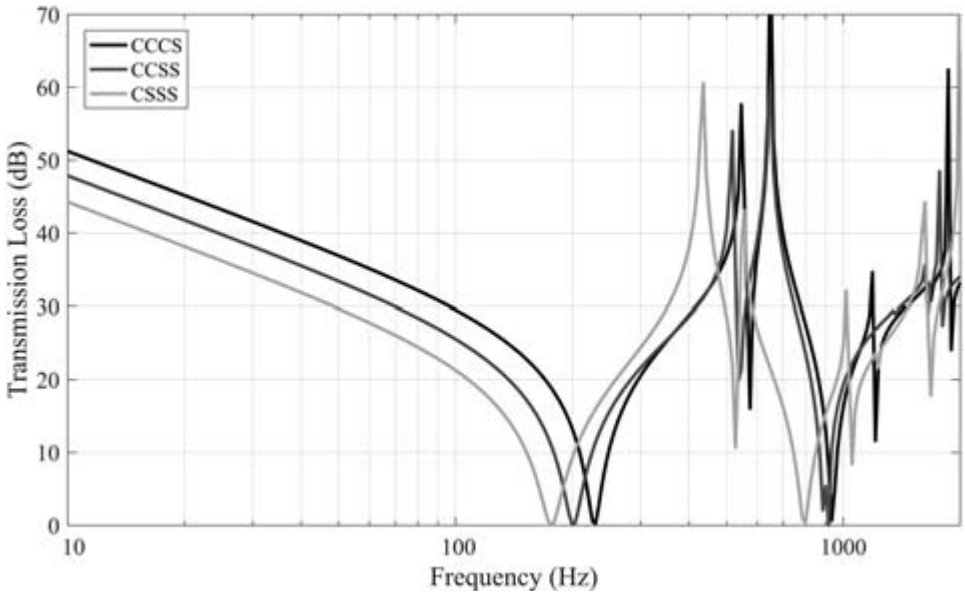

Figure 9. Transmission loss through plate–mass systems belonging to Class B as a function of frequency

the peak transmission loss of the fully clamped case. This presents a problem for MAM designers, as the improper installation of these structures can markedly reduce efficiency in the frequency range they may be designed to attenuate. Precisely how important the boundary conditions are relative to other design parameters is captured in Figure 10, which shows that the effect of different mounting conditions can more strongly influence the transmission loss curve than the effects of an added mass. In this figure, the first and second transmission loss

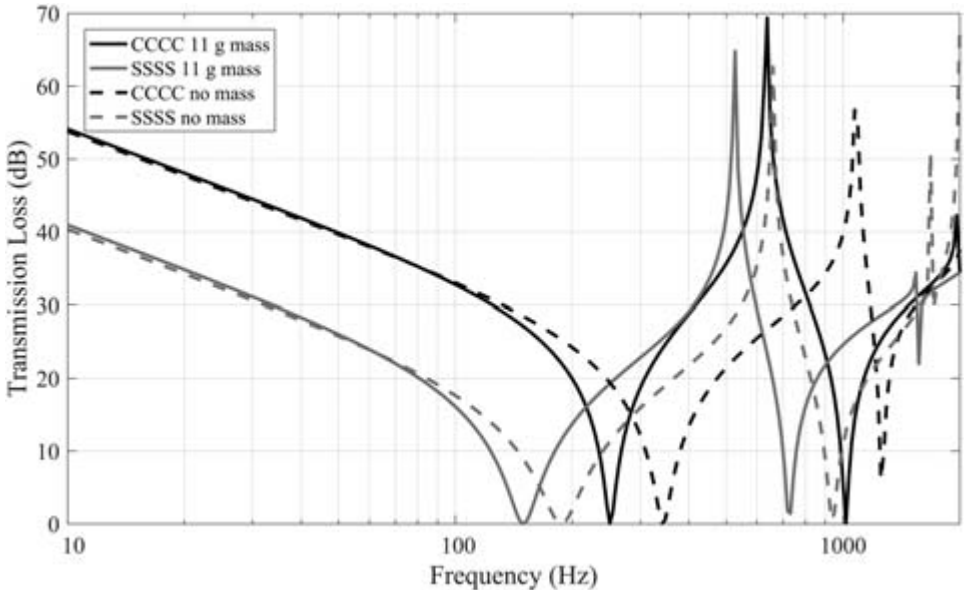

Figure 10. Transmission loss through plates with and without mass loading, demonstrating the relative importance of boundary conditions

Please cite the article as: W Edwards, CM Chang, G McKnight, and SR Nutt **"Analytical model for low-frequency transmission loss calculation of plates with arbitrary mass loading",** J Vibration & Acoust (2019) DOI:10.1115/1.4042927

minima for an $SSSS_A$ plate with bonded 0.011 kg mass (150 Hz) relocate to a higher frequency when the edges are clamped (250 Hz) than when the mass is removed (187 Hz).

3. CONCLUSIONS

An analytical model was developed and validated to describe acoustic transmission loss through plate structures with attached rigid masses of arbitrary number, shape, weight, and location under various boundary conditions. A point matching approach was used to approximate the coupling force between a Kirchhoff–Love plate and attached rigid mass as a finite set of discrete point forces. Admissible functions given by natural mode shapes of single-span beams with appropriate boundary conditions were used to solve the resulting equations of motion using a modal expansion approach. The representative linear eigenvalue problem was presented and its components were defined for rectangular plates with any combination of clamped and pinned boundaries. The effective surface mass density of the plate was calculated as a function of excitation frequency for normally incident acoustic waves and used to determine the transmission loss through the metamaterial. Edge mounting conditions of the platelike metamaterial were shown to strongly influence the acoustic performance of the structure, with asymmetric mounting conditions giving rise to additional transmission loss maxima and minima when compared with symmetric boundaries. Boundary conditions also strongly influenced the off-modal transmission properties.

The model presented offers improved utility over previous work by allowing prediction of the antisymmetric plate motion, while inheriting the efficiency and accuracy of the numerical scheme presented by Langfeldt et al. [12]. The model can be implemented using standard linear algebra methods and solved efficiently using existing techniques and packages, but its accuracy is limited to acoustic frequencies below the frequency corresponding to a wavelength equal to the characteristic length of the plate. The model can accommodate any

Please cite the article as: W Edwards, CM Chang, G McKnight, and SR Nutt **"Analytical model for low-frequency transmission loss calculation of plates with arbitrary mass loading",** J Vibration & Acoust (2019) DOI:10.1115/1.4042927

number of masses placed arbitrarily on the plate; however, masses are assumed to be ridged. This assumption is not limiting for masses that are sufficiently small or stiff; however, the model is not well suited to capturing the behavior of large, thin, compliant mass loading.

The practical significance of this work is threefold. First, we provide a theoretical demonstration that the same phenomena giving rise to favorable transmission loss properties exhibited by MAMs can also be inspired in stiffer materials systems. This result opens the design space of locally resonant, two-dimensional acoustic metamaterials. Second, we demonstrate the critical importance of boundary conditions and explore their influence on platelike acoustic metamaterial performance. Finally, the efficient analytical tools presented here give engineers and acousticians a toolbox for streamlining and optimizing the design and frequency response of plate-type acoustic metamaterials.

References

[1] Toyoda, M., Kugo, H., Shimizu, T., and Takahashi, D., 2008, "Effects of an Air-Layer Subdivision Technique on the Sound Transmission Through a Single Plate," J. Acoust. Soc. Am., 123(2), pp. 825–831.
[2] Yang, Z., Mei, J., Yang, M., Chan, N. H., and Sheng, P., 2008, "Membrane-Type Acoustic Metamaterial With Negative Dynamic Mass," Phys. Rev. Lett., 101(20), 204301.
[3] Liu, Z., Zhang, X., Mao, Y., Zhu, Y. Y., Yang, Z., Chan, C. T., and Sheng, P., 2000, "Locally Resonant Sonic Materials," Science, 289(5485), pp. 1734–1736.
[4] Naify, C. J., Chang, C. M., McKnight, G., and Nutt, S., 2010, "Transmission Loss and Dynamic Response of Membrane-Type Locally Resonant Acoustic Metamaterials," J. Appl. Phys., 108(11), 114905.
[5] Zhang, Y., Wen, J., Xiao, Y., Wen, X., and Wang, J., 2012, "Theoretical Investigation of the Sound Attenuation of Membrane-Type Acoustic Metamaterials," Phys. Lett. A, 376(17), pp. 1489–1494.
[6] Naify, C. J., Chang, C., McKnight, G., and Nutt, S., 2011, "Transmission Loss of Membrane-Type Acoustic Metamaterials With Coaxial Ring Masses," J. Appl. Phys., 110(12), 124903.
[7] Naify, C. J., Chang, C.-M., McKnight, G., and Nutt, S. R., 2012, "Scaling of Membrane-Type Locally Resonant Acoustic Metamaterial Arrays," J. Acoust. Soc. Am., 132(4), pp. 2784–2792.
[8] Ingard, U., 1954, "Transmission of Sound Through a Stretched Membrane," J. Acoust. Soc. Am., 26(1), pp. 99–101.
[9] Kornhauser, E. T., and Mintzer, D., 1953, "On the Vibration of Mass-Loaded Membranes," J. Acoust. Soc. Am., 25(5), pp. 903–906.
[10] Cohen, H., and Handelman, G., 1957, "On the Vibration of a Circular Membrane With Added Mass," J. Acoust. Soc. Am., 29(2), pp. 229–233.

Please cite the article as: W Edwards, CM Chang, G McKnight, and SR Nutt **"Analytical model for low-frequency transmission loss calculation of plates with arbitrary mass loading",** J Vibration & Acoust (2019) DOI:10.1115/1.4042927

[11] Chen, Y., Huang, G., Zhou, X., Hu, G., and Sun, C.-T., 2014, "Analytical Coupled Vibroacoustic Modeling of Membrane-Type Acoustic Metamaterials: Membrane Model," J. Acoust. Soc. Am., 136(3), pp. 969–979.
[12] Langfeldt, F., Gleine, W., and von Estorff, O., 2015, "Analytical Model for Low-Frequency Transmission Loss Calculation of Membranes Loaded With Arbitrarily Shaped Masses," J. Sound Vib., 349, pp. 315–329.
[13] Xin, F. X., and Lu, T. J., 2009, "Analytical and Experimental Investigation on Transmission Loss of Clamped Double Panels: Implication of Boundary Effects," J. Acoust. Soc. Am., 125(3), pp. 1506–1517.
[14] Kim, H.-S., Kim, S.-R., Lee, S.-H., Seo, Y.-H., and Ma, P.-S., 2016, "Sound Transmission Loss of Double Plates With an Air Cavity Between Them in a Rigid Duct," J. Acoust. Soc. Am., 139(5), pp. 2324–2333.
[15] Chen, Y., Huang, G., Zhou, X., Hu, G., and Sun, C.-T., 2014, "Analytical Coupled Vibroacoustic Modeling of Membrane-Type Acoustic Metamaterials: Plate Model," J. Acoust. Soc. Am., 136(6), pp. 2926–2934.
[16] Inman, D. J., 2014, Engineering Vibration, Pearson Education, Inc., Upper Saddle River, NJ.
[17] Fahy, F. J., and Gardonio, P., 2007, Sound and Structural Vibration: Radiation, Transmission, and Response, Academic Press, Oxford, UK.
[18] Belvins, R. D., 2016, Formulas for Dynamics, Acoustics, and Vibration, John Wiley & Sons, Ltd, Chichester, West Sussex.

Please cite the article as: W Edwards, CM Chang, G McKnight, and SR Nutt **"Analytical model for low-frequency transmission loss calculation of plates with arbitrary mass loading",** J Vibration & Acoust (2019) DOI:10.1115/1.4042927